Ferritin nanoconjugates guide trastuzumab brain delivery to promote an antitumor response in murine HER2 + breast cancer brain metastasis

Marta Sevieri [a], Serena Mazzucchelli [a], Linda Barbieri [b], Stefania Garbujo [b], Stephana Carelli [c,d], Arianna Bonizzi [e], Federica Rey [c,d], Camilla Recordati [f,g], Matteo Recchia [f,g], Raffaele Allevi [a], Leopoldo Sitia [a], Carlo Morasso [e], Pietro Zerbi [h], Davide Prosperi [b], Fabio Corsi [a,e,*], Marta Truffi [e,**,1]

[a] Department of Biomedical and Clinical Sciences, Università degli Studi di Milano, via G.B. Grassi 74, 20157 Milan, Italy
[b] Department of Biotechnology and Biosciences, University of Milano-Bicocca, P.zza della Scienza 2, 20126 Milano, Italy
[c] Pediatric Clinical Research Center "Romeo ed Enrica Invernizzi", Department of Biomedical and Clinical Science, University of Milan, 20157 Milan, Italy
[d] Center of Functional Genomics and Rare Diseases, Department of Pediatrics, Buzzi Children's Hospital, Milano, Italy
[e] Istituti Clinici Scientifici Maugeri IRCCS, via Maugeri 4, 27100 Pavia, Italy
[f] Mouse and Animal Pathology Laboratory, Fondazione Unimi, viale Ortles 22/4, 20139 Milano, Italy
[g] Dipartimento di Medicina Veterinaria e Scienze Animali, Università di Milano, via dell'Università 6, 26900 Lodi, Italy
[h] Anatomia Patologica, ASST Santi Paolo e Carlo, via Pio II, 3, Milano, Italy

ARTICLE INFO

ABSTRACT

Brain metastasis (BM) represents a clinical challenge for patients with advanced HER2 + breast cancer (BC). The monoclonal anti-HER2 antibody trastuzumab (TZ) improves survival of BC patients, but it has low central nervous system penetrance, being ineffective in treating BM. Previous studies showed that ferritin nanoparticles (HFn) may cross the blood brain barrier (BBB) through binding to the transferrin receptor 1 (TfR1). However, whether this has efficacy in promoting the trans-BBB delivery of TZ and combating BC BM was not studied yet. Here, we investigated the potential of HFn to drive TZ brain delivery and promote a targeted antitumor response in a murine model of BC BM established by stereotaxic injection of engineered BC cells overexpressing human HER2. HFn were covalently conjugated with TZ to obtain a nanoconjugate endowed with HER2 and TfR1 targeting specificity (H-TZ). H-TZ efficiently achieved TZ brain delivery upon intraperitoneal injection and triggered stable targeting of cancer cells. Treatment with H-TZ plus docetaxel significantly reduced tumor growth and shaped a protective brain microenvironment by engaging macrophage activation toward cancer cells. H-TZ-based treatment also avoided TZ-associated cardiotoxicity by preventing drug accumulation in the heart and did not induce any other major side effects when combined with docetaxel. These results provided in vivo demonstration of the pharmacological potential of H-TZ, able to tackle BC BM in combination with docetaxel. Indeed, upon systemic administration, the nanoconjugate guides TZ brain accumulation, reduces BM growth and limits side effects in off-target organs, thus showing promise for the management of HER2 + BC metastatic to the brain.

1. Introduction

Breast cancer (BC) overexpressing the human epidermal growth factor receptor 2 (HER2) represents 15–20% of breast malignancies and it is particularly prone to form distant metastases [1,2]. The advent of HER2-targeting agents has prolonged survival in patients with advanced disease, but the prevention and management of brain metastases (BM) still poses unique clinical challenges [3,4]. BM represents a catastrophic event that portends a poor prognosis and, once established, lack an effective cure. This is mainly due to an inconsistent penetrance of anti-HER2 therapies across the blood–brain barrier (BBB), a highly-selective filter that surveys the entry of substances to the brain and hinders drug efficacy in case of BM [5–7]. Despite efforts in the development of more permeable drugs, nowadays do not yet exist recommended first-line treatments with demonstrated capability to prevent brain recurrence, and trastuzumab (TZ) remains the first therapeutic option in HER2 + disease [8–10]. New generation of antibody-drug conjugates, which combine HER2-specific antibody backbone with a potent cytotoxic payload, has shown a reduction of metastases in advanced HER2 + BC. However, there was no decrease in the risk of BM as the first site of relapse [11,12]. Moreover, these potent drugs are associated with non-negligible toxicity and adverse events that raise questions on their use [13].

Based on these observations, it is of utmost importance to develop more effective and less toxic strategies to control, and ultimately prevent, brain involvement in HER2 + BC, especially using appropriate models to ensure the achievement of reliable preclinical data for a straightforward clinical translation.

Human Ferritin (HFn) is a versatile and biocompatible nanoparticle holding several advantages for cancer application [14–17]. Among many properties, HFn is able to cross the BBB exploiting the Transferrin Receptor 1 (TfR1), overexpressed in the BBB endothelium [18–20]. The trans-BBB permeability of HFn was successfully demonstrated both by our and other group research work by using a fluorescent tracer payload as a proof of principle or drugs loaded inside HFn cavity [21–23]. More recently, we demonstrated that HFn can bind brain endothelial cells in a dose-dependent manner and favour the trans-BBB crossing of curcuminoids through a BBB cellular model [24]. We also demonstrated the feasibility of HFn use as a vector for the trans-BBB delivery of high molecular weight compounds, such as therapeutic monoclonal antibodies [25]. Ferritin nanoconjugates based on the covalent conjugation of TZ on HFn surface (H-TZ) were designed to preserve both HER2-targeting specificity and the capability of HFn subunits to bind TfR1. As reported in a previous paper, as-designed H-TZ were able to translocate across a transwell BBB system in vitro, preserving their target specificity and antitumor activity toward HER2 + BC cells in vitro [25].

Aim of this study was to investigate the potential of H-TZ to enhance the trans-BBB permeation in vivo, and to promote targeted antitumor response for an effective brain protection. To this aim, we established a mouse experimental model of BC-derived BM, which combined specific molecular features of engineered BC cells, overexpressing the human HER2 and the luciferase transgene, with a controlled intracranial implantation, for the generation of in vivo-trackable BM sensitive to TZ. After model characterization, we assessed the capability of H-TZ to reach the brain tumor upon a systemic administration, and investigated the impact on tumor growth of H-TZ combined with the cytotoxic drug docetaxel. As standard of care, a group of mice was administered with free TZ, equally dosed, combined with docetaxel. The effect of treatment on microglia was also analyzed as the brain microenvironment is an important mediator of effective antitumor response. Finally, we investigated side effects generally associated to chemotherapy based on anti-HER2 *plus* taxanes, to gain insights into potential toxicity triggered by H-TZ treatment.

2. Methods

2.1. Cell line

The murine breast tumor cell line D2F2/E2, stably expressing the human HER2 receptor, was originally obtained from prof. Wei Zen-Wei (Wayne University). Cells were transduced with RediFect Red-FLuc-Puro Lentiviral Particles (Perkin Elmer, Boston, MA, USA) following the manufacturer's instructions. The lentiviral particles carry the luciferase reporter transgene (Luc) fused with a selectable marker that confers resistance to the antibiotic puromycin. Transduced cells were selected by applying a selective medium containing puromycin (1 μg/mL). Then, selected puromycin resistant clones were expanded in culture to assay for expression of luciferase. D2F2/E2-Luc cells were maintained at 37 °C in a humidified atmosphere containing 5% CO_2 in high glucose Dulbecco's modified Eagle's medium (DMEM) supplemented with 2 mM L-glutamine, 10% fetal bovine serum (FBS), 1% non-essential amino acids, 1% penicillin/streptomycin, G418 (0.8 mg/mL) and puromycin (250 ng/mL). Cells were passaged at sub-confluence using trypsin/EDTA and amplified for 2 weeks before implant in mice. All cell culture reagents were purchased by Euroclone (Italy).

2.2. Murine model of breast cancer brain metastasis

Nude BALB/c female mice (6–8 weeks old) were purchased by Charles River Laboratories (Calco, Italy), group housed in IVC cages with free access to sterile food and water and allowed to acclimate for one week before tumor implant. Animals were handled in accordance with an experimental study approved by the Italian Ministry of Health (aut. N. 6/2017-PR). Mice were anesthetized using isoflurane and positioned in a stereotactic apparatus (2Biological Instruments). A linear skin incision was made over the bregma. Then, D2F2/E2-Luc cells (1 ×10^5) were suspended in cold serum-free DMEM medium and injected into the mouse brain (4 μL total volume, speed rate 2 μL min^{-1}) with a 10 μL Hamilton syringe under constant isoflurane anesthesia (1.5%). Stereotactic coordinates were 1 mm right from the bregma, 3 mm depth from the skull. After injection, the skin was closed with absorbable stitches, and tramadol (30 mg kg^{-1}) was administered by intraperitoneal (IP) injection to relieve post-operative pain. Mice wellness was monitored daily, and tumor growth was followed by bio-luminescence imaging (BLI) at the specified time-points before euthanasia. BLI signals were acquired with the IVIS Lumina II imaging system (Perkin Elmer) 5 min after IP injection of D-luciferin (150 μg kg^{-1}, Perkin Elmer) with an exposure time of 10 s. Images were quantified using regions of interest analysis of individual mice and the signal was expressed as total BLI Counts.

2.3. Preparation of H-TZ nanoconjugate

HFn nanoparticles were produced and purified as previously reported [26]. HFn were conjugated to the anti-HER2 mAb trastuzumab (TZ, Ogivri, Mylan) according to a protocol already described by our group to obtain a 1:1 HFn/TZ ratio per nanoparticle [25]. Briefly, A PEG-based heterobifunctional crosslinker (MW PEG ≈ 5000 Da), bearing one N-hydroxysuccinimidyl ester (NHS) and one maleimide (Mal) group, was used to anchor TZ on HFn in a two steps reaction. Next, reaction products were isolated by size exclusion chromatography (SEC-FPLC), which identifies distinct peaks for the protein complex and each unreacted species. The reaction product (H-TZ) was characterized by SDS-PAGE, western blot and dynamic light scattering analysis.

2.4. In vitro cell-binding assays

D2F2/E2-Luc cells (5 ×10^5 cells/tube) were collected and incubated for 2 h at 4 °C with H-TZ (0.01, 0.1, 1, 10, 100 μg/mL) or with corresponding concentrations of free TZ diluted in PBS with 0.3% BSA. After

incubation, cells were washed thrice with PBS and incubated for 15 min at RT with anti-human Alexa Fluor 488 secondary antibody (1 µg/tube, Invitrogen) diluted in PBS with 2% BSA, 2% goat serum. Labelled cells were washed thrice with PBS and analyzed in triplicates using CytoFLEX flow cytometer (Beckman Coulter). Acquisition was performed on 20,000 events, after gating on singlets viable cells. Untreated cells immunodecorated with the secondary antibody only were used to set the region of positivity.

For the kinetics assay, cells (5×10^4) were seeded in 12-well plates and incubated for 1 h at 37 °C with 100 µg/mL of H-TZ or corresponding concentration of TZ diluted in the culture medium. Cells were then washed thrice with PBS and provided with fresh culture medium. After 1, 4, 24, 48, 72 h cells were detached with Trypsin/EDTA, labelled with anti-human Alexa Fluor 488 secondary antibody and acquired with CytoFLEX as described above.

2.5. Intracranial injection of TZ

To check efficacy of TZ in murine HER2 + BC BM, 1 µL of TZ (0.08 and 0.8 mg Kg^{-1}, corresponding to 1% and 10% of the standard parenteral dose, respectively) was mixed with 3 µL of cell suspension (1 $\times 10^5$ cells) and immediately injected intracranially using the stereotactic apparatus as described above. As control, 1 µL of saline was used instead of TZ in a group of mice. The BLI analysis was used to evaluate the therapeutic efficiency from 4 to 14 days after tumor cells were implanted. Mice were sacrificed at day 7 (n = 6/group) and day 14 (n = 6/group) post tumor implant, and brains were then dissected on ice and processed for analysis.

2.6. Systemic therapy studies

For the systemic therapy study, mice were randomly assigned into four groups (n = 15 mice per group). The first group of mice was treated with a combination of TZ (Ogivri, Mylan) and docetaxel (Dtx, Accord) as a standard of care treatment scheduled for HER2 + metastatic BC. The second group received H-TZ (equivalent TZ dose) and Dtx. The third group received Dtx alone. A fourth group received saline solution as placebo treatment and was considered the untreated control. Free TZ or nanoformulated H-TZ were administered IP at 8 mg kg^{-1} every 3 days for 2 weeks, with the first injection performed 30 min before tumor implant and then repeated after 4, 7 and 11 days. Dtx (15 mg kg^{-1}) was intravenously injected via the tail vein at 4 days post-tumor implant. The BLI analysis was used to evaluate the therapeutic efficiency of different treatments from 4 to 14 days after tumor cells were implanted. Nine mice per group were sacrificed at day 7 post-tumor implant, brains were dissected on ice and either fixed in paraformaldehyde (PFA, 4%) to assess TZ accumulation into the tumor (n = 3/group), or snap frozen to extract RNA (n = 3/group), or fixed in formalin to perform histological evaluations (n = 3/group). The remaining mice (n = 6 per group) were sacrificed at day 14 post-tumor implant to gain insights into the potential long term toxicity effects of H-TZ treatment.

2.7. Tumor histology assessment

For histological examination, mice brains were fixed in 10% neutral buffered formalin for a minimum of 24 h. Three coronal sections (obtained by using Adult Mouse Brain Slicer Matrix BSMAS005–1, Zivic Instruments, USA) were routinely processed for paraffin embedding, sectioned at 4 µm thickness, stained with hematoxylin-eosin (H&E, Mayer's haematoxylin, cat. No. C0302; Eosin G, cat. No. C0362, Diapath, Martinengo, Bergamo, Italy), and evaluated under a light microscope.

At day 7 p.i. a semi-quantitative grading system considering distribution (1 = focal; 2 = multifocal) and size (0 = absent; 1 = diameter < 500 µm; 2 = 500 µm < diameter < 2000 µm; 3 = diameter > 2000 µm) of the tumors in different brain regions (parenchyma, sub-ventricular zone, ventricles, leptomeninges) was applied. A histology score (HS) was obtained multiplying the distribution by the size in each region in the three coronal sections. Then, for each animal, a total HS was calculated summing all the HS. Histopathological evaluation was performed in a blind fashion (i.e., without information about the treatment groups).

2.8. Immunofluorescence and confocal microscopy

After PFA fixation, brain tissues were embedded in optimal cutting temperature (OCT) compound (VWR International) and frozen at − 80 °C. Then, 10 µm-thick cryosections were cut, washed with PBS, permeabilized with 0.1% Triton X-100 for 5 min and incubated with blocking solution (2% goat serum, 2% BSA in PBS) for 2 h at RT. TZ was visualized in sections using anti-human Alexa Fluor 546 secondary antibody (Invitrogen) diluted 1:300 in blocking buffer and incubated overnight at 4 °C. HER2 was stained on adjacent slices with anti-HER2/ErbB2 (29D8, Cell Signaling Technology, Inc.) diluted 1:200 in blocking buffer and incubated overnight at 4 °C as a primary detection antibody, and goat anti-rabbit Alexa Fluor 546 as secondary antibody (Invitrogen, 1:300) for 2 h at RT. Nuclei were stained with DAPI (0.1 µg/mL for 15 min) and slides were mounted in ProLong Gold antifade reagent (Invitrogen).

For astrocytes analysis, 4 µm-thick FFPE brain tissue slides were deparaffinized with Xilene (AppliChem), rehydrated with graded ethanol, equilibrated in PBS, blocked with 2% goat serum, 2% BSA, 0.01% Triton X-100 for 1 h at RT, incubated with anti-GFAP antibody (PRB-571 C, Covance) diluted 1:1000 in 1% goat serum, 1% BSA, 0.01% Triton X-100 for 3 h at RT and then stained with goat anti-rabbit Alexa Fluor 546 secondary antibody (Invitrogen, 1:300) overnight at 4 °C. Nuclei were stained with DAPI (0.1 µg/mL for 15 min) and slides were mounted in ProLong Gold antifade reagent (Invitrogen) for microscopic acquisition.

Images of the tumor were acquired at 20 × magnification with SP8 confocal microscope (Leica) using the Tile Scan function of the Leica LAS X Navigator. Quantification of the fluorescence signal was performed on single scans by measuring the integrated density in single-channel calibrated images and calculating the mean from multiple images. All analyzed images had the same area and resolution was of 512 × 512 pixels. Analysis of captured images was performed using Fiji software.

2.9. Immunohistochemistry

For immunohistochemistry (IHC), brain sections underwent deparaffinization and heat induced epitope retrieval (HIER) in a water bath for 30 min at 100 °C (Dewax and HIER Buffer H, Thermo Scientific Lab Vision, cat. No. TA-999-DHBH). The slides were rinsed in PBS and placed in an autostainer (Lab Vision® Autostainer 4^{80}S–^{2}D Thermo fischer scientific) after application of PapPen (Liquid Daido Sangyo Co., Ltd.). Endogenous peroxidase activity was blocked by incubating sections with 3% H$_2$O$_2$ for 10 min. Slides were rinsed, incubated with PBS containing 10% normal goat serum for 30 min at room temperature to prevent nonspecific background staining and then incubated for 1 h at room temperature with the primary antibody rabbit polyclonal anti-Iba1 (marker of microglia, ab178846, Clone:EPR16588, Abcam). Sections were subsequently rinsed in PBS and incubated with a biotinylated secondary antibody (goat anti-rabbit, Vector Laboratories, USA, cat. No. BA-1000) and labelled by the avidin-biotin-peroxidase procedure (VECTASTAIN® Elite ABC-Peroxidase Kit Standard, Vector Laboratories, USA, cat. No.PK-6100). The immunoreaction was visualized with 3,3′-diaminobenzidine substrate (DAB, Peroxidase DAB Substrate Kit, Vector Laboratories, USA, cat. No. SK-4105). Sections were counterstained with Mayer's haematoxylin (Diapath, Martinengo (BG), Italy, cat. No. C0302), dehydrated in a graded alcohol series and coverslipped with resinous mounting medium.

Immunostained sections were digitalized using the NanoZoomer S60 Digital slide scanner (Hamamatsu, C13210–01) at the Unitech Nolimits
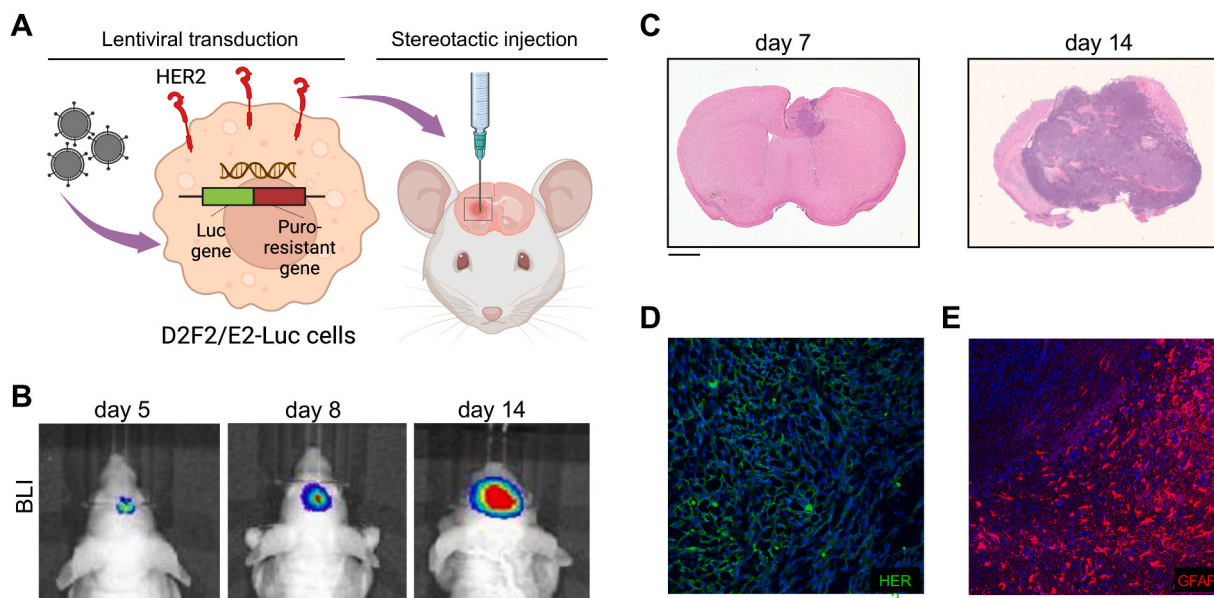
Fig. 1. Murine model of BC-derived HER2 + BM. A) D2F2/E2 BC cells expressing human HER2 were engineered by lentiviral transduction to express luciferase reporter and puromycin-resistant gene, and injected in the brain of mice by stereotactic injection. B) BLI was assessed in vivo at different time-points up to 14 days post-tumor implant. C) Hematoxylin and eosin staining was performed on FFPE sections from the frontotemporal part of brain dissected from mice at 7 and 14 days post-tumor implant. Scale bar = 1 mm. Expression of HER2 on tumor cells (D, green) and GFAP on reactive astrocytes (E, red) was assessed by immunofluorescence on brain tumor sections at 14 days post-implant. Nuclei were stained with DAPI (blue). Scale bar = 100 μm.

(UNIMI, Milano) and images were captured by using the NDP.view2 Viewing software (Hamamatsu, U12388- 01). The % of Iba1-positive immunostained area and the number of Iba1-positive cells were evaluated using the ImageJ analysis program (https://imagej.nih.gov/ij/) in 3 20x microscopic fields randomly selected within the tumor (intra-tumoral), and surrounding the tumor (peri-tumoral). A mean value of the microscopic fields was then calculated for each sample.

2.10. Cytokines analysis by qRT-PCR

Mice brains (n = 3/group) were dissected on ice and cut with a scalpel to obtain the frontotemporal part of the right hemisphere, corresponding to the brain fragment containing the tumor (¼ of the total brain). Brain fragments were snap frozen in liquid nitrogen immediately after dissection and preserved at – 80 °C. Total RNA was extracted using TRIZOL® reagent (Thermo Fisher Scientific) following the manufacturer's instructions, and then quantified with the Multiskan GO spectrophotometer (Thermo Fisher Scientific). RNA was retro-transcribed using the iScriptTM Reverse Transcription Supermix for RT-qPCR (Bio-Rad) kit following manufacturer's instructions. Real-Time PCR was performed with the CFX Connect Real-Time PCR System (Bio-Rad) using Optimum qPCRMaster Mix with SYBR® Green (Genespin). The NCBI's Primer-BLAST tool was used to design primers. Gene expression was calculated using the 2^{-ddCt} method. GAPDH was used as endogenous control. The list of primers used in this study is reported in Supporting Table S1.

2.11. Heart lysate and western blot

Hearts were dissected from treated mice (n = 3/group) at day 14 post tumor implant, snap frozen in liquid nitrogen and stored at – 80 °C until usage. Frozen tissues were homogenized in water (10% w/v), lysed for 30 min at 4 °C in 20 mM Tris HCl pH 7.6, 150 mM NaCl, 1 mM EDTA, 1% Triton X-100, 1% glycerol, 1 mM Na_3VO_4, 10 mM NaF, Protease Inhibitor Cocktail, 1 mM PMSF, and centrifuged to discard cell debris. Protein content was determined by Bradford assay. A total of 35 μg of lysate was loaded on SDS-PAGE (12% acrylamide) and transferred onto PVDF membrane (Sigma-Aldrich). Membranes were blocked in TBS supplemented with 5% nonfat dry milk and 0.1% Tween 20 (Sigma-Aldrich) for 1 h and then incubated overnight at 4 °C with goat anti-human antibody conjugated with horseradish peroxidase (#GTX26759, Tebu-bio) diluted 1:2000 in TBS with 0.1% Tween 20. Vinculin was used as loading control protein. Chemiluminescence reaction was developed with Clarity Western ECL Substrate (Biorad) and images were acquired with the Chemidoc System (Biorad).

2.12. Transmission electron microscopy (TEM)

From 3 mice/group, heart tissue was excised after the sacrifice and fixed in 2.5% glutaraldehyde in 0.1 M phosphate buffer, pH 7.2 at 4 °C. After rinsing with PBS, specimens were post-fixed in 1.5% osmium tetroxide for 2 h, dehydrated by 50%, 70%, 90%, and 100% EtOH and embedded in epoxy resin (PolyBed 812 Polysciences Inc.). Ultrathin sections were cut with an ultramicrotome (Ultracut E (Reichert-Jung)), stained with uranyl acetate and lead citrate and examined by TEM (Tecnai Spirit, FEI). Mitochondria quantification and mitochondria morphometric measurements were performed using ImageJ software as previously described [27].

2.13. Assessment of liver and kidneys functionality

Before euthanasia, blood was collected from the retro-orbital plexus of anesthetized mice and collected in EDTA-coated tubes (Becton Dickinson). Plasma was isolated by centrifugation at 2000g for 10 min at RT, followed by a second centrifugation at 2500g for 10 min at 4 °C to remove platelets. Liver and kidneys functionality were assessed after 2 weeks of treatment by measuring the plasma levels of AST and ALT (for liver), urea and creatinine (for kidneys). The following kits were used according to the manufacturer's protocols: QuantiChrom™ Urea Assay Kit, QuantiChrom™ Creatinine Assay Kit, EnzyChrom™ Aspartate Transaminase Assay Kit and EnzyChrom™ Alanine Transaminase Assay Kit (BioAssay Systems).

2.14. Statistical analysis

Statistical analysis was done using GraphPad Prism 6 (San Diego, CA,
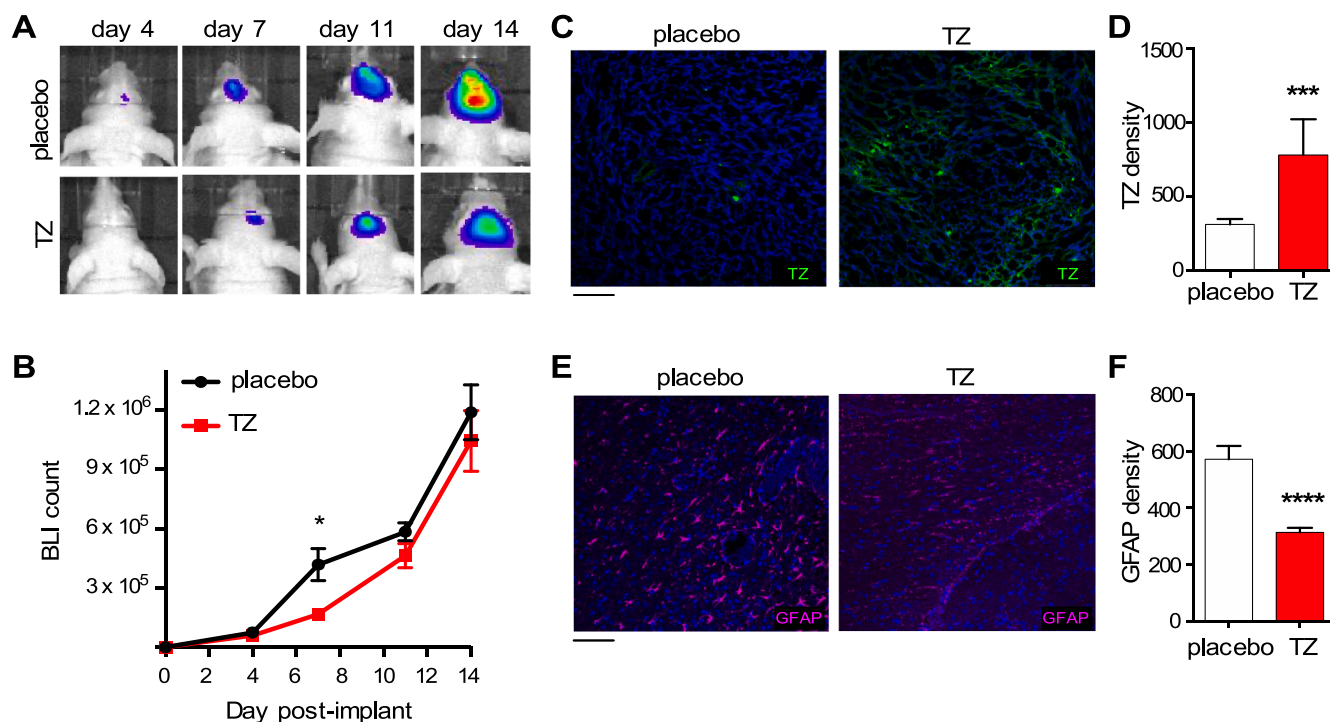
Fig. 2. Antitumor effect of TZ injected intracranially. A) In vivo bio-luminescence of tumors treated with placebo or with intracranial TZ at different time-points post-tumor implant. B) Mean tumor growth curves were drafted based on the BLI counts of TZ-treated (red) and untreated (black) mice, measured at 4, 7, 11 and 14 days post-tumor implant. Data are means ± SEM (n = 6/group). *p = 0.011 unpaired t-test. Brains were dissected at day 7 post-tumor implant and tissue sections were stained with anti-human secondary antibody to visualize TZ (C) or with anti-GFAP antibody to analyze reactive astrocytes (E). Nuclei were stained with DAPI (blue). Scale bar = 100 μm. D) Mean TZ signal intensity was quantified on single-channel images taken within the tumor of 3 mice per group; at least 3 fields of view, all with the same area, were analyzed per each tumor. Data are means ± SEM. * **p = 0.0003 Mann Whitney test. F) Mean GFAP signal intensity was quantified on single-channel images taken in the peri-tumoral region of 2 mice per group; at least 10 fields of view, all with the same area, were analyzed per each tumor. Data are means ± SEM. * ** *p < 0.0001 Mann Whitney test.

USA). The Student t-test or the non-parametric Mann Whitney test were used when comparing two groups in case of normal and non-normal distribution of the data, respectively. The Kruskal-Wallis test followed by Dunnet's multiple comparison's tests was applied when comparing more than two groups. Statistical significance was set at p-value < 0.05.

3. Results and Discussion

### 3.1. Experimental model of BC-derived BM

In order to study the potential of H-TZ nanoconjugates to promote TZ brain delivery in vivo, we first set up a suitable experimental model of BC-derived BM. We took advantage of the murine BC cell line D2F2/E2, which overexpressed human HER2 and has been previously used by us for therapeutic studies involving TZ [27]. Before implant in mice, the cells were engineered by transduction with RediFect lentiviral particles to make them express the luciferase transgene (Luc) fused to the puromycin resistance gene as a selection marker. Stable clones were selected for resistance to puromycin and stability of bioluminescent signal, and then intracranially injected via stereotactic technique to generate an orthotopic model of brain tumor derived from HER2 + BC (Fig. 1A). This model has the advantages to (i) overexpress the human HER2 protein thus displaying the specific ligand for TZ anchoring; (ii) be easily visualized in vivo by bio-luminescence imaging (BLI) thanks to the stable Luc expression; (iii) more closely mimic the biological interactions between the tumor and the brain microenvironment since the tumor cells originate from the same species of the host.

After tumor implant, the BLI analysis revealed engraftment of the cells and rapid tumor growth in the brain of mice between 4 and 14 days post-injection (Fig. 1B). Tumor histology, assessed at 7 and 14 days post-injection, showed that the tumor expanded around the injection site and

localized in the frontotemporal part of the right hemisphere invading the brain parenchyma (Fig. 1C). HER2 expression was clearly detected by immunofluorescence on the membrane of tumor cells grown for 2 weeks in the mouse brain (Fig. 1D). Images with higher magnification displaying in detail the localization of HER2 have been included in the Supporting Information (Fig. S1). The tumor also induced alteration in the brain microenvironment, triggering the formation of a glial reaction around the boundaries of tumor mass. Staining for GFAP identified a multitude of reactive astrocytes in the brain parenchyma surrounding the tumor (Fig. 1E). Images with higher magnification displaying in detail the localization of GFAP are reported in the Supporting Information (Fig. S2). GFAP overexpression is typical of the profound remodeling and shaping of astrocytes in certain pathological conditions in which homeostasis has been compromised [28,29]. Reactive astrocytes have been extensively described also in the context of BC BM [30,31]. They are activated by the tumor and in turn play a prominent role in promoting the growth of cancer cells by paracrine cytokine signaling [32–34]. Being important players in BM formation, reactive astrocytes represented a key step of characterization of our experimental model, further supporting how it recapitulates the physiopathological interplay between the tumor and the brain microenvironment.

3.2. Sensitivity to TZ

To prove whether the experimental model of BC-derived BM was sensitive to TZ, we performed a pilot study by injecting a small dose of TZ intracranially, simultaneously to the inoculation of tumor cells. In this setup TZ was locally administered, so no issue was imposed regarding BBB permeability, and the direct sensitivity of the tumor to TZ could be analyzed. To choose an appropriate dosage, we reasoned that only a very small amount of a drug normally administered via parenteral
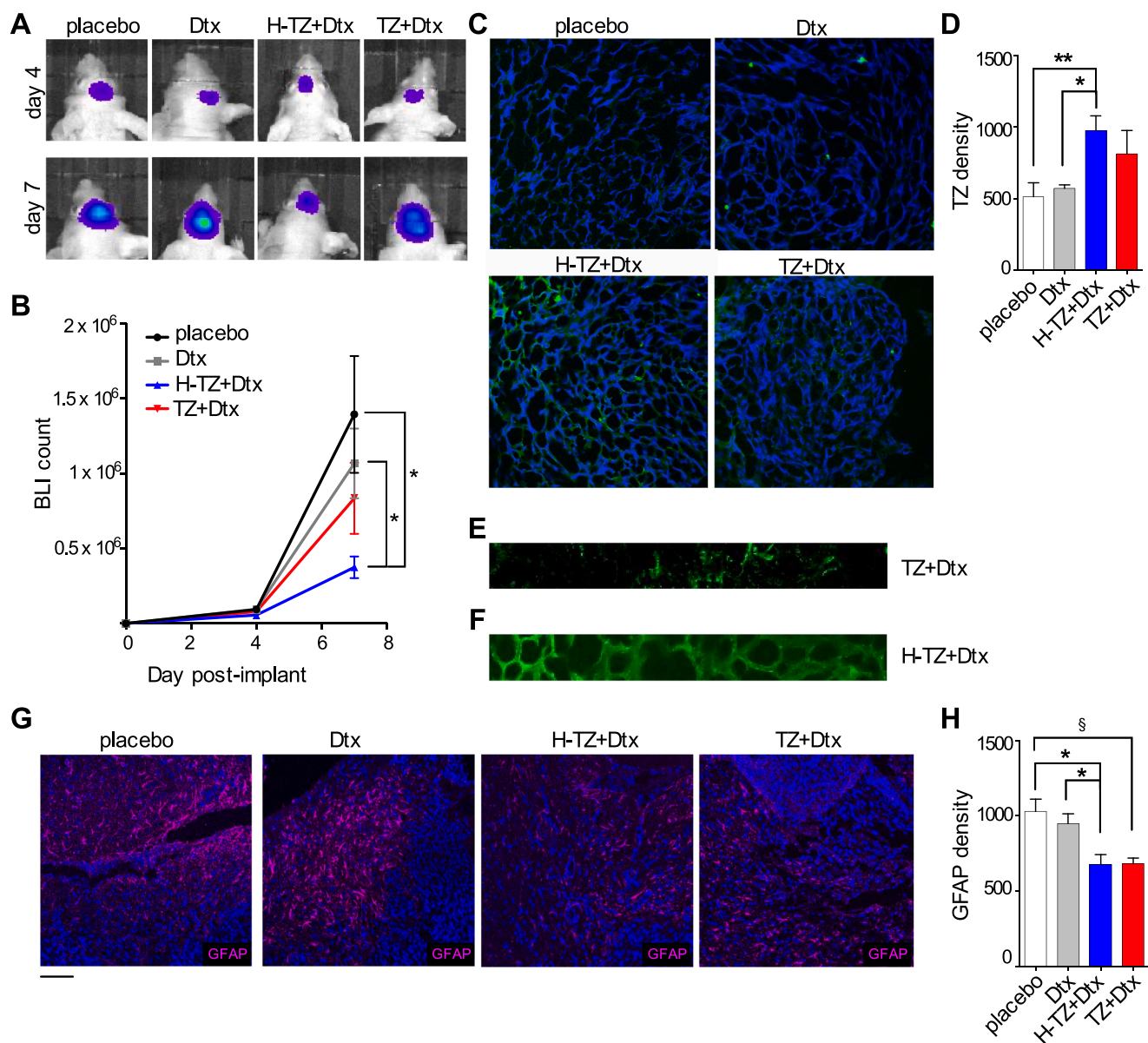
Fig. 3. Systemic treatment with free TZ or H-TZ in combination with Dtx. A) In vivo bio-luminescence of tumors treated with placebo, Dtx, H-TZ+Dtx or TZ+Dtx at 4 and 7 days post-tumor implant. B) Mean tumor growth curves were drafted based on the BLI counts of untreated mice (black) or mice treated with Dtx (grey), H-TZ+Dtx (blue), TZ+Dtx (red). Data are means ± SEM (n = 15/group). *p = 0.01 unpaired t-test. C) Brains were dissected at day 7 and stained with anti-human secondary antibody to visualize TZ (green). Nuclei were stained with DAPI (blue). D) Mean TZ signal intensity was quantified on single-channel images taken within the tumor of 2 mice per group; at least 3 fields of view, all with the same area, were analyzed per each tumor. Data are means ± SEM. *p = 0.016; * *p = 0.006 Kruskal Wallis test. E-F) High magnification of single channel images from representative tumors treated with H-TZ+Dtx (E) or TZ+Dtx (F). G) Immunofluorescence analysis of GFAP (magenta) on brain tissue slices at day 7. Nuclei were stained with DAPI (blue). Scale bar = 100 μm. H) Mean GFAP signal intensity was quantified on single-channel images taken in the peri-tumoral region of 2 mice per group; at least 7 fields of view, all with the same area, were analyzed per each tumor. Data are means ± SEM. *p = 0.008; §p = 0.006 Kruskal Wallis test.

injection can reach the brain [35]; therefore, we tested two doses of TZ corresponding to 10% and 1% of the dose that is recommended for therapeutic purpose in mice, i.e. 0.8 and 0.08 mg Kg^{-1}, respectively. Results from a pilot study demonstrated that both dosages significantly slowed down tumor growth to a similar extent (see Supporting Fig. S3), hence we chose the lowest effective dose for the further phase of the study. TZ administration was performed through a stereotactic injection together with the tumor cells, to ensure that the drug came into contact with its target. After 4, 7, 11 and 14 days post-injection, the proliferation of viable tumor cells was monitored in vivo through BLI, thanks to stable expression of Luc (Fig. 2A). Tumors treated with 0.08 mg Kg^{-1} of TZ showed a significant reduction of growth at 7 days post-treatment as compared to untreated tumors (p = 0.011, Fig. 2B).

To investigate the effects of TZ at a cellular level, mouse brains were dissected at day 7 and analyzed by immunofluorescence. The analysis allowed to detect the presence of TZ bound to tumor cells in the group of TZ-treated mice (Fig. 2C-D). TZ treatment also triggered a reduced astrocytic reaction in the brain parenchyma, as a consequence of the reduced tumor growth (Fig. 2E). Images with higher magnification are included in the Supporting Information (Figs. S4–S5). While GFAP overexpression was observed on astrocytes in the placebo group, a lower intensity of GFAP was measured in TZ-treated brains, as shown by quantitative image analysis on brain sections (Fig. 2F). These data proved sensitivity of the model to TZ, and indicated a 7-day time window to detect drug efficacy on tumor progression. At 11 days post-treatment, the aggressiveness of the tumor overcame the

pharmacological effect of the drug and the tumor started growing again, requiring the ethical sacrifice of the animals at day 14 in both placebo and TZ groups (Fig. 2B). This observation confirmed the aggressiveness of BM and underlined the need to intervene early in order to achieve pharmacological efficacy.

3.3. H-TZ brain delivery and antitumor activity

Considering that local intracranial administration of drugs is extremely invasive and often not easily translatable to the clinic, especially in the case of many brain injuries localized in different areas of the brain, we conceived a bio-nanoconjugate suitable for the active delivery of TZ across the BBB via a systemic administration, thus avoiding intracranial injection. The nanoconjugate was designed to achieve covalent conjugation of TZ antibody on the surface of HFn nanoparticles through a heterobifunctional PEG linker. The nanoconjugate's features, including particle size and morphology, were previously published [25] and reported in Supplementary Information (Fig. S6). Upon conjugation, the antibody was readily accessible for HER2 targeting. At the same time, HFn maintained its natural capability to bind TfR1, a receptor overexpressed on many solid tumors and on the BBB endothelium. The capability of H-TZ to successfully cross the BBB preserving its targeted specificity and antitumor activity toward HER2 + BC cells was proved in vitro and reported in a previously published paper [25]. Here, we decided to challenge it in vivo, assessing the brain distribution of nanoformulated TZ vs. free TZ upon systemic IP administration in a murine model of BM.

This experimental design reproduced a first-line treatment used in clinics for HER2 + metastatic BC, based on anti-HER2 *plus* a taxane [36, 37]. Since in clinical practice TZ is never used as a single agent but always administered in combination with cytotoxic drugs, we decided to combine it with docetaxel (Dtx), administered 4 days post-tumor implant. Moreover, it allowed to simultaneously study brain distribution and therapeutic performance of the nanodrug. Given that the described therapeutic scheduling never involves the administration of TZ alone, by respecting the principle of reduction for animal welfare, we did not consider it necessary to include a group treated with H-TZ only. Animals were sacrificed 7 days post-implant to explore drug efficacy in a relevant therapeutic window.

Results obtained by in vivo BLI revealed that H-TZ+Dtx treatment induced a significant reduction of the tumor growth 7 days post-tumor implant as compared to both placebo (p = 0.01) and mice treated with Dtx alone (p = 0.01, Fig. 3A-B). By contrast, mice treated with free TZ+Dtx did not achieve a statistically significant effect on the tumor growth (p = 0.21 vs. placebo; p = 0.49 vs. Dtx), confirming inefficacy of traditional chemotherapy toward BM. Immunofluorescence on brain tumor sections demonstrated a clear and bright signal corresponding to TZ in the brain of mice treated with H-TZ+Dtx (Fig. 3C). Images with higher magnification are included in the Supporting Information (Fig. S7). Quantification of the signal intensity further confirmed that H-TZ reached the brain and successfully accumulated in the tumor (p = 0.006 vs. placebo; p = 0.016 vs. Dtx) to a greater extent than free TZ did (p = 0.27 vs placebo; p = 0.20 vs Dtx) (Fig. 3D). Some TZ was retrieved also in the brain of mice treated with the free standard formulation TZ+Dtx. However, free TZ was detected as a weak pinpoint signal on very few cells only, as observed in the high magnification image (Fig. 3E). In case of H-TZ+Dtx, instead, the signal appeared uniformly distributed on the membrane of cancer cells (Fig. 3F), suggesting a more stable targeting of HER2 + tumor cells by the nanoformulation vs. free TZ.

Immunofluorescence analysis also revealed that treatment with H-TZ+Dtx triggered a reduced astrocytic reaction in the brain parenchyma, as indicated by analysis of GFAP marker (Fig. 3G). For magnified images, refer to the Supporting Information (Fig. S8).

Signal quantification confirmed that tumors treated with H-TZ+Dtx were associated to reduced GFAP expression as compared to placebo and
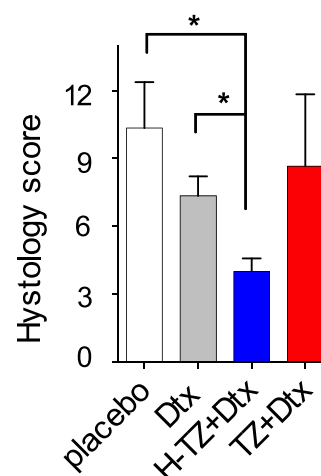

Fig. 4. Histological assessment in H&E-stained brain sections at 7 days post-implant. A total histology score was obtained by semi-quantitative grading system in different treatment groups. Data are means ± SEM (n = 3/group). *p = 0.04 one-tail Mann Whitney test.

Dtx (p = 0.008). Also, in TZ+Dtx group a reduced density of GFAP staining was observed on astrocytes with respect to placebo (p = 0.006), but not with respect to Dtx alone (Fig. 3H), further demonstrating a limited contribution of free TZ in shaping an antitumor response.

Then, we assessed the histopathological features of the brain tumor by performing H&E staining on multiple sequential brain sections. A pathologist, blinded to the treatment conditions of each animal, analyzed the brain slides to evaluate tumor histology. The results showed that the lesions recovered in the brain of mice treated with H-TZ+Dtx were reduced as compared to placebo and Dtx groups (p = 0.04, Fig. 4). Instead, the total histology score in TZ+Dtx group was not significantly different (p = 0.35 vs. placebo and Dtx), confirming inefficacy of standard free drug administered systemically in the context of BM.

Overall, these data indicated a relevant contribution of H-TZ in driving TZ brain accumulation and targeting of cancer cells. Moreover, they showed that treatment with H-TZ+Dtx shaped a less aggressive and slower tumor progression, when administered systemically in the early phase of BM formation.

3.4. Microglia recruitment and effect on neuroinflammation

Highly malignant brain tumors are characterized by large numbers of microglia/macrophages that influence cancer progression, being able to suppress or support the malignancy depending on their activation and polarization state [38,39]. In this study we investigated whether H-TZ+Dtx treatment had an impact on the density and distribution of Iba1, a marker of microglia/macrophages. Iba1-positive area was found increased in the peri-tumoral regions of mice treated with H-TZ+Dtx (Fig. 5A), while the number of Iba1-positive cells remained similar. Quantitative analysis of Iba1 immunostaining is shown in Supporting Table S2. By correlation analysis between Iba1 positivity and the total histology score in matched animals, we observed that reduced development tumor was associated with an increase in the Iba1-positive area (r = −0.85, p = 0.004). Therefore, enhanced efficacy of the H-TZ+Dtx treatment was strongly associated with increased activation of macrophages around the tumor. This is likely due to a mechanism mediated by the interaction between macrophage receptors and antibodies bound to the cells. Once engaged by the antibody, activated macrophages trigger an antibody-dependent cancer cell killing, contributing to the antitumor response [40,41]. We thus hypothesized that, by guiding TZ brain accumulation, H-TZ not only allowed direct interaction with HER2 signaling, but also triggered a sustained activation of macrophages
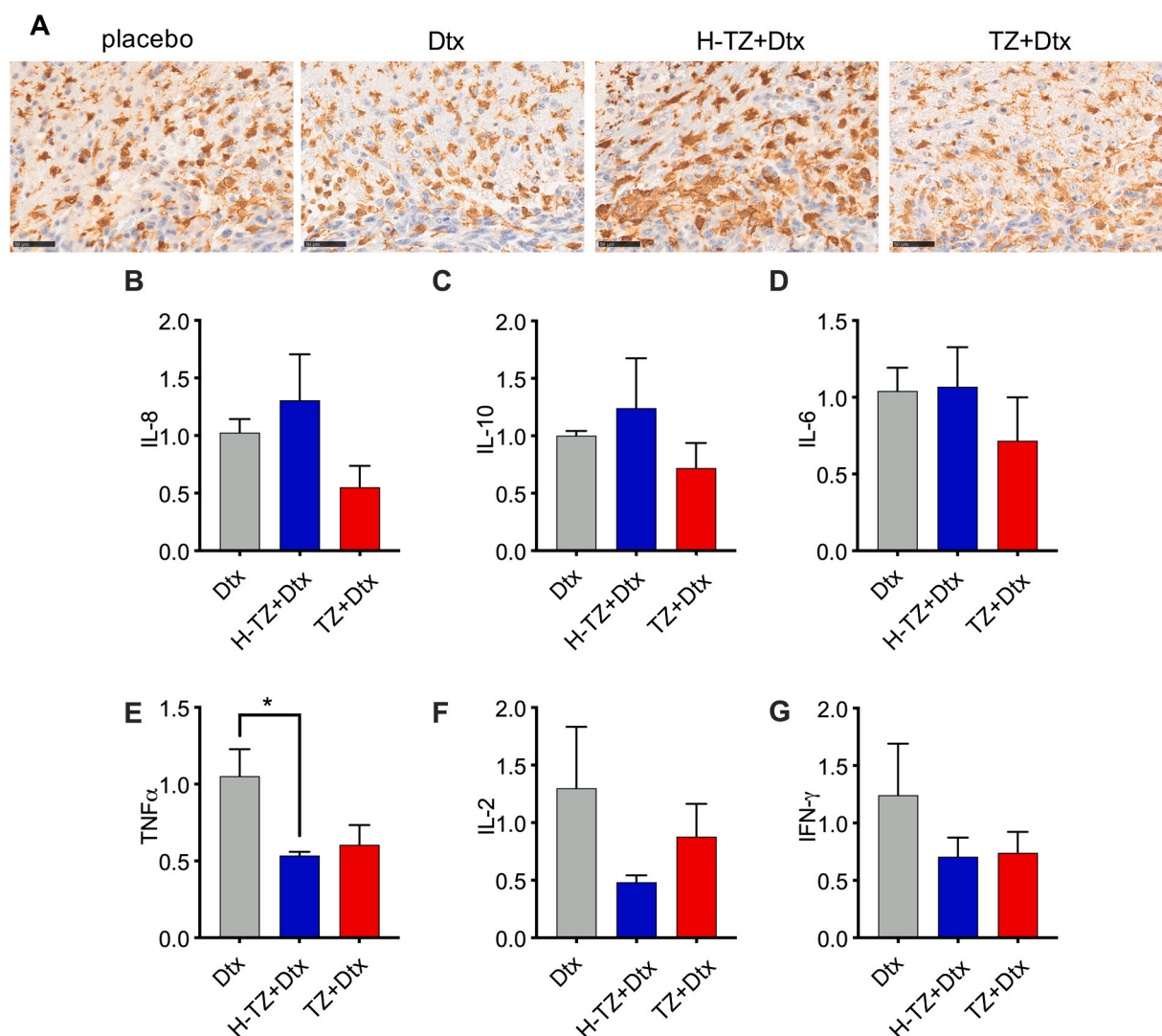
Fig. 5. Investigation of pro- and anti- inflammatory biomarker in mouse brains. A) Immunohistochemistry of Iba1 (brown signal) in the peri-tumoral region. Scale bar = 50 μm. B-E) Real Time qPCR was performed on brain tumor specimens to measure expression of IL-8 (B), IL-10 (C), IL-6 (D), TNFα (E), IL-2 (F) and IFN-γ (G) in the treatment groups. Results are expressed as RNA fold change. Dtx group was used for normalization. Data are means ± SEM, each animal was analyzed in duplicate (n = 6/group).

toward the cancer cells to shape a protective microenvironment against the tumor.

To further explore the impact of the treatment on the brain microenvironment, we measured the expression of cytokines, important mediators of neuroinflammation. Brains treated with H-TZ+Dtx were compared with those treated with Dtx alone or with the combination TZ+Dtx. Protective cytokines, like IL-8 and IL-10, were analyzed because it has been shown that they can be released by macrophages actively engaged in antibody-dependent cancer cell killing [42,43]. Their expression in brain tissues showed a trend toward increase in H-TZ+Dtx group as compared to TZ+Dtx group (Fig. 5B-C). Despite this was only a trend with no statistical significance, the increased expression of IL-8 and IL-10 could be associated to the enhanced Iba1 positivity observed by immunohistochemistry, and further supported the antitumor activity of H-TZ in the brain. The expression of the IL-6 proinflammatory cytokine remained unchanged (Fig. 5D). We decided to investigate the expression of other proinflammatory cytokines (TNFα, IL-2 and IFN-γ) highlighting relevant differences. We observed a significant decrease in TNFα expression in H-TZ+Dtx group (Fig. 5E), along with the decrease in IL-2 (Fig. 5F) and IFN-γ (Fig. 5G) in the same condition. Indeed, IL-10 was found to downregulate the expression of

some proinflammatory cytokines, hence these results may correspond to the increase of IL-10 found in H-TZ+Dtx group. TNFα decrease is particularly interesting considering that this cytokine can be a double edge sword in cancer pathology, and its decrease was shown to enhance therapeutic efficacy [44,45]. Moreover, IFN-γ was recently found to promote metastatic lesions in the brain, suggesting that its decrease could indicate an efficacy of therapy.

3.5. H-TZ anchoring to target tumor cells

Given the higher antitumor response achieved by H-TZ+Dtx treatment as compared to free TZ+Dtx, we hypothesized that the nanoconjugate, endowed with a double specificity for HER2 and TfR1, could promote a more stable anchoring to the target tumor cells, therefore conditioning the tumor more extensively. To test this hypothesis, we analyzed the performance of H-TZ in a binding assay with D2F2/E2-Luc cells in vitro. Equal concentrations of nanoformulated or free TZ were incubated for 2 h at 4 °C with the cells and then analyzed by flow cytometry to visualize TZ bound on the cells. Both H-TZ and TZ were able to efficiently bind the cells in a dose-dependent manner, with more than 99% of the cells found positive at a drug concentration as low as
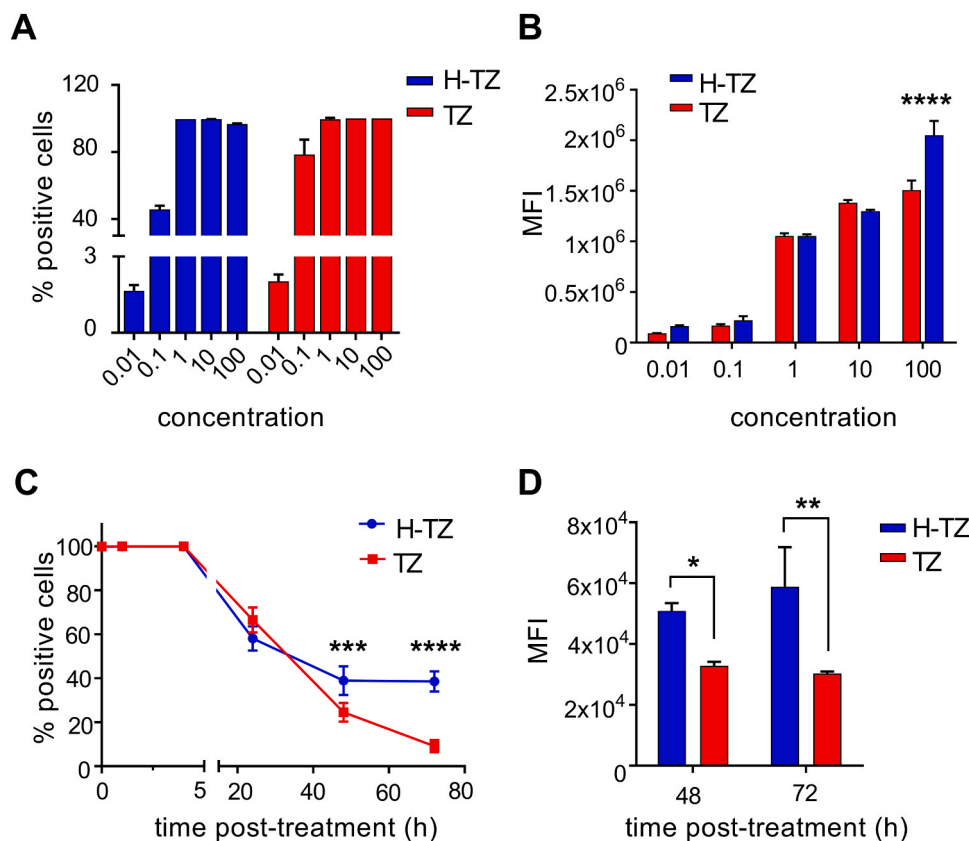
Fig. 6. In vitro cell binding assay. A) Binding of H-TZ and TZ incubated at 0.01, 0.1, 1, 10, 100 µg/mL with tumor cells. B) Mean fluorescence intensity (MFI) of H-TZ or TZ bound to the cells. * ** *p = 0.005 unpaired t-test. C) Persistence of H-TZ and TZ on the cells after 1, 4, 24, 48, 72 h post-treatment. Statistics by 2-way ANOVA. D) MFI of H-TZ or TZ bound to the cells after 48 and 72 h post-treatment. Statistics by 2-way ANOVA. All data are means ± SD (n = 3).

1 µg/mL (Fig. 6A). By increasing the dose, the mean fluorescence intensity (MFI) of the positive events increased, meaning that more H-TZ or TZ molecules attached to the same cell (Fig. 6B). At 100 µg/mL, a higher MFI was observed for H-TZ as compared to free TZ (p = 0.005). This result likely suggests advantage of the nanoconjugate, which can overcome the saturation of single HER2 target by engaging TfR1 in the binding, thus increasing the upper limit of molecules per cell. Instead, the MFI for free TZ did not increase further between 10 and 100 µg/mL, indicating that even increasing the drug dosage no more receptors could be engaged in binding.

Then we performed a kinetic assay by incubating the cells with an equal concentration of H-TZ or free TZ and measuring for how long they persist on the cell surface (Fig. 6C). The percentage of TZ-positive cells was maintained high after 1 and 4 h, then decreased down to 24.6% and 9.1% at 48 and 72 h, respectively. In the case of H-TZ, the percentage of positive cells also decreased over time, but a significantly higher percentage of cells, i.e. 38.9% and 38.5%, was still positive after 48 h and 72 h, respectively. To further document the longer on-cell persistence of H-TZ over free TZ, we analyzed the MFI of the events collected at 48 and 72 h. We found that MFI related to H-TZ was significantly higher than that of TZ (Fig. 6D), suggesting that at the indicated time-points there were on average more H-TZ particles exposed on the cells as compared to TZ.

These data demonstrated that H-TZ may trigger a more stable and lasting anchoring to the cancer cells as compared to free TZ, thus extending the residence time and the drug load at the target site. This in vitro observation further supported what was found in vivo, i.e. a stronger signal of H-TZ stably and uniformly distributed on cancer cells than free TZ (Fig. 3D). Moreover, it suggested that the advantage of H-TZ nanoconjugate may not only rely on active HFn-mediated trans-BBB delivery of TZ, but also on the persistence of TZ anchored to the tumor

cells, further prolonging its pharmacological efficacy.

3.6. H-TZ do not induce cardiotoxicity and relevant off-target effects

Once analyzed the therapeutic effect, we explored whether H-TZ could be associated with long-term systemic toxic effects. To this aim we scheduled a complete therapeutic cycle, by repeating the IP injection of H-TZ twice weekly for 2 weeks, and combining it with a single intravenous injection of Dtx. As control, free TZ was administered instead of H-TZ in a group of mice, and combined with Dtx to mimic standard of care treatment.

We monitored tumor growth by BLI for the entire duration of the treatment. The tumor growth curve showed that mice treated with H-TZ+Dtx had a significant reduction of the tumor growth at day 7 (p = 0.043 vs. placebo and Dtx; p = 0.037 vs. TZ+Dtx) and day 11 (p = 0.039 vs. placebo and Dtx), further supporting the pharmacological potential of the nanoconjugate. At day 14 post-implant, the benefit of the nanotherapy was not statistically significant anymore, but an evident trend towards reduced tumor growth was still observed in the H-TZ+Dtx as compared to the other groups. By contrast, treatments with TZ+Dtx or Dtx alone did not achieve effective reduction of the tumor growth at any of the examined time-point (Fig. 7A), being ineffective against BM.

At day 14 post-tumor implant, animals were sacrificed and we investigated the effect of the treatments on major known drawback associated to TZ-based chemotherapy, i.e. cardiotoxicity [46]. Heart tissues were analyzed by transmission electron microscopy to explore the ultrastructural features of cardiomyocytes at the end of the treatment. The images showed severe ultrastructural changes in the TZ+Dtx group, with swollen mitochondria and severe cristae disruption (Fig. 7B). This phenotype indirectly indicated impaired functionality of
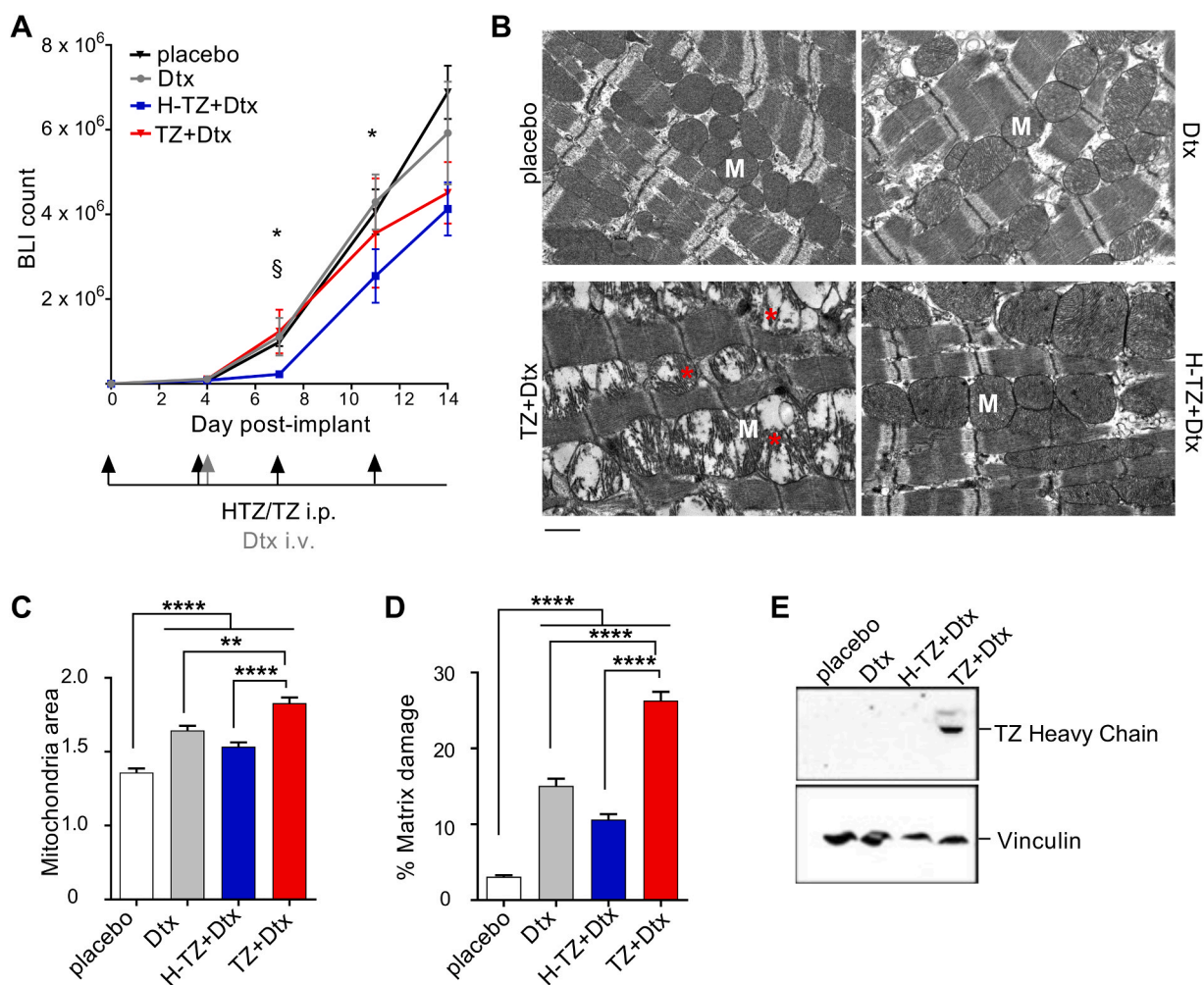
Fig. 7. Toxicity analysis. A) Tumor growth curve of untreated mice (black) or mice treated with Dtx (grey), H-TZ+Dtx (blue), TZ+Dtx (red). Data are means ± SEM (n = 6/group). Day 7: *p = 0.043 H-TZ+Dtx vs. placebo/Dtx; §p = 0.037 H-TZ+Dtx vs. TZ+Dtx. Day 11: *p = 0.039 H-TZ+Dtx vs. placebo/Dtx, unpaired t-test. B) Representative TEM images of heart tissues excised at day 14 post-treatment (n = 3/group). It is evident a significant difference in terms of both mitochondrial area (M) and matrix damage (*) in the TZ+Dtx group in comparison with the other groups. Scale bar = 1 μm. C) Analysis of mean mitochondria area expressed in μm². D) Analysis of the percentage of damaged matrix mitochondrial area. Data are means ± SEM. Quantification of mitochondria area and area occupied by the matrix were performed on at least 10 images/group, measuring at least 100 mitochondria/sample. * *p < 0.01; * ** *p < 0.0001 Kruskal-Wallis test. E) Western blot analysis of heart excised at the end of treatment and lysed to quantify TZ. Vinculin was used as loading control protein.
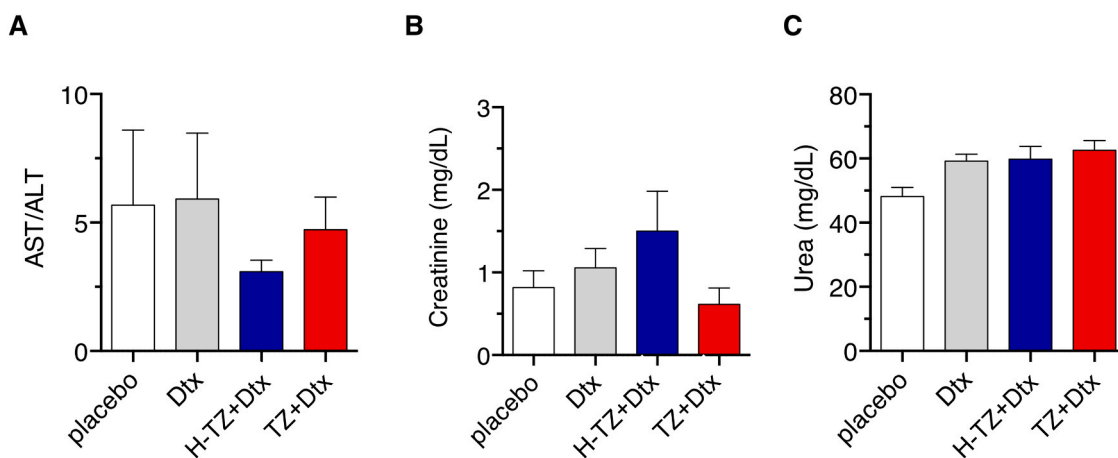
Fig. 8. Assessment of liver and kidney functionality. Aspartate to alanine aminotransferase ratio (AST/ALT) (A), Creatinine (B) and Urea (C) levels measured in the plasma collected from placebo and treated mice were used as biomarkers of liver and kidney disfunction, respectively (n = 8 /group). Statistical analysis confirmed no significant differences among the groups.

the mitochondria in oxidative phosphorylation and consequent heart failure in meeting adequate energy demand. Alterations in mitochondria area observed in the TZ+Dtx group were significantly marked in comparison to the other treatments (Fig. 7C), and this is likely due to a compensatory mechanism for deficiency in mitochondrial cristae, which were replaced by matrix (Fig. 7D). Mitochondrial ultrastructure was severely compromised by the addition of TZ in the TZ+Dtx group as compared to Dtx alone. By contrast, H-TZ+Dtx treatment did not induce further detrimental effects on either the mitochondria area or the percentage of matrix, as compared to Dtx alone, indicating a great potential advantage of the H-TZ nanoconjugate in protecting toward TZ-induced cardiotoxicity (Fig. 7C-D). The absence of additive alterations in cardiac mitochondria was explained by the fact that no TZ accumulation was found in heart tissue lysates upon treatment with H-TZ+Dtx (Fig. 7E). By contrast, a TZ-specific band was detected by western blot in the heart of mice treated with TZ+Dtx, suggesting accumulation of the free drug, but not the nanoformulated drug, in this organ. Based on these observations, we reasoned that the nanoconjugate guided the biodistribution of the drug differently, by achieving enhanced TZ brain delivery and reducing accumulation in the heart. In another paper from our group, HFn nanoformulation was found to reduce heart accumulation and protect against cardiotoxicity associated to the chemotherapy doxorubicin [47], further supporting our observation and confirming the advantage of HFn-based nanodrugs in terms of heart protection.

We further assessed the systemic toxicity profile of H-TZ-based treatment by looking at liver and kidney functionalities. In fact, previous data on HFn demonstrated that a prevalent fraction of nanoparticles that were not captured by the tumor distributed in the liver and were rapidly sequestered by the kidneys for urinary excretion [47]. Plasma levels of aspartate transaminase (AST) and alanine transaminase (ALT), and urea and creatinine were analyzed as markers of liver and kidney function, respectively. Our results showed that AST/ALT ratios in all the treatment groups were comparable to the placebo and in the range of reference (Fig. 8A) [48–50]. Urea (Fig. 8B) and creatinine (Fig. 8C) dosage did not show significant alterations upon treatment with H-TZ+Dtx as compared to placebo and Dtx alone, confirming the overall safety of H-TZ nanoconjugate.

Finally, we looked at blood count results to explore any potential side effect of H-TZ-based cancer treatment detectable in peripheral blood. No remarkable alterations were observed in the levels of white blood cells (WBC), red blood cells (RBC), and platelets (PLT). Hemoglobin concentration (HGB) was also measured, and did not highlight a clinical picture of anemia in any of the treated animals (Supporting Table S3).

No lesions were observed by histopathology in other off target organs (Supplementary Fig. S9).

4. Conclusions

Achieving a curative treatment of HER2 + BC BM is an unsolved clinical challenge [51]. The anti-HER2 antibody TZ improves survival of BC patients and controls the systemic disease, but it has low BBB permeability, being ineffective at treating BM [4,52]. Our prior findings obtained in vitro support H-TZ as a promising approach for the treatment of brain tumors by virtue of their ability to cross the BBB and achieve cytotoxic effect against tumor cells [21,25]. The present study, aimed at investigating the potential of H-TZ to enhance the trans-BBB permeation in vivo, demonstrated that HFn is able to actively guide TZ delivery to the brain upon systemic administration in a murine model of HER2 + BM. H-TZ bound cancer cells efficiently and stably, reducing tumor growth in vivo and shaping an antitumor response in combination with Dtx. H-TZ-based therapy also triggered activation of microglia toward cancer cells and induced alterations in the neuroinflammation, further supporting enhanced activity as compared to free TZ. These results have translational relevance, as they demonstrate that active delivery of TZ to the brain by HFn nanoparticles may exert pharmacological activity in the context of HER2 + BC BM, which is a

great promise in the field. HFn drives TZ distribution to the brain and reduces major harmful accumulation in off-target organs, like the heart, thus reducing side effects and undesired toxicity generally associated with treatments currently used in clinics.

In conclusion, we first described the in vivo potential of HFn-based TZ nanoconjugates able to vehicle effective TZ to the brain and tackle BC-derived BM without major toxic effects. As perspective, H-TZ nanoconjugates deserve attention as they could be exploited for a prophylactic treatment of HER2 + advanced BC aimed to condition the tumor and timely shape a protective brain microenvironment.

Ethics statement

Animals were handled in accordance with an experimental study approved by the Italian Ministry of Health (aut. N. 6/2017-PR). The procedures followed were in accordance with the ethical standards of the WMA Statement on Animal Use in Biomedical Research.

CRediT authorship contribution statement

MS: Conducted experiments in vivo and contributed to data analysis and data curation; **SM**, **AB:** contributed to in vivo/ex vivo analyses and data curation. **SC**, **FR:** performed RNA analysis; **CR**, **MR**, **PZ:** contributed to histology and immunohistochemistry; **LB**, **SG**, **DP:** produced the nanoconjugate; **RA:** performed TEM analysis; **LS**, **CM:** Contributed to data analysis and interpretation. **FC**, **MT:** contributed to the conception and design of the work and supervised the study. All authors contributed to drafting the work or revising it critically for important intellectual content. All authors read and approved the final manuscript.

Declaration of Competing Interest

The authors declare that they have no known competing financial interests or personal relationships that could have appeared to influence the work reported in this paper.

Data Availability

Data will be made available on request. Raw data are available at https://doi.org/10.13130/RD_UNIMI/IG8LEA.

Appendix A. Supporting information

Supplementary data associated with this article can be found in the online version at doi:10.1016/j.phrs.2023.106934.

References

[1] H. Hosseini, M.M.S. Obradović, M. Hoffmann, et al., Early dissemination seeds metastasis in breast cancer, Nature 540 (2016) 552–558.

[2] S. Loibl, L. Gianni, HER2-positive breast cancer, Lancet 389 (2017) 2415–2429.

[3] S. Dawood, K. Broglio, A.U. Buzdar, G.N. Hortobagyi, S.H. Giordano, Prognosis of women with metastatic breast cancer by HER2 status and trastuzumab treatment: an institutional-based review, J. Clin. Oncol. J. Am. Soc. Clin. Oncol. 28 (2010) 92–98.

[4] A.S. Zimmer, A.E.D. Van Swearingen, C.K. Anders, HER2-positive breast cancer brain metastasis: A new and exciting landscape, Cancer Rep. 5 (2022), e1274.

[5] M. Kim, S.H. Kizilbash, J.K. Laramy, et al., Barriers to effective drug treatment for brain metastases: a multifactorial problem in the delivery of precision medicine, Pharm. Res. 35 (2018) 177.

[6] S. Rathi, J.I. Griffith, W. Zhang, et al., The influence of the blood-brain barrier in the treatment of brain tumours, J. Intern Med 292 (2022) 3–30.

[7] N.J. Abbott, Blood-brain barrier structure and function and the challenges for CNS drug delivery, J. Inherit. Metab. Dis. 36 (2013) 437–449.

[8] K.A. Gelmon, F.M. Boyle, B. Kaufman, et al., Lapatinib or trastuzumab plus taxane therapy for human epidermal growth factor receptor 2-positive advanced breast cancer: final results of NCIC CTG MA.31, J. Clin. Oncol. J. Am. Soc. Clin. Oncol. 33 (2015) 1574–1583.

[9] S.M. Swain, J. Baselga, D. Miles, et al., Incidence of central nervous system metastases in patients with HER2-positive metastatic breast cancer treated with pertuzumab, trastuzumab, and docetaxel: results from the randomized phase III study CLEOPATRA, Ann. Oncol. J. Eur. Soc. Med Oncol. 25 (2014) 1116–1121.

[10] I.E. Krop, N.U. Lin, K. Blackwell, et al., Trastuzumab emtansine (T-DM1) versus lapatinib plus capecitabine in patients with HER2-positive metastatic breast cancer and central nervous system metastases: a retrospective, exploratory analysis in EMILIA, Ann. Oncol. J. Eur. Soc. Med Oncol. 26 (2015) 113–119.

[11] G. von Minckwitz, C.-S. Huang, M.S. Mano, et al., Trastuzumab emtansine for residual invasive HER2-positive breast cancer, New Engl. J. Med. 380 (2019) 617–628.

[12] E. Ferraro, J.Z. Drago, S. Modi, Implementing antibody-drug conjugates (ADCs) in HER2-positive breast cancer: state of the art and future directions, Breast Cancer Res. 23 (2021), 84.

[13] S. Modi, C. Saura, T. Yamashita, et al., Trastuzumab deruxtecan in previously treated HER2-positive breast cancer, New Engl. J. Med. 382 (2020) 610–621.

[14] F. Mainini, A. Bonizzi, M. Sevieri, et al., Protein-based nanoparticles for the imaging and treatment of solid tumors: the case of ferritin nanocages, a narrative review, Pharmaceutics 13 (2021) 2000.

[15] M. Truffi, L. Fiandra, L. Sorrentino, M. Monieri, F. Corsi, S. Mazzucchelli, Ferritin nanocages: A biological platform for drug delivery, imaging and theranostics in cancer, Pharm. Res 107 (2016) 57–65.

[16] M. Liang, K. Fan, M. Zhou, et al., H-ferritin-nanocaged doxorubicin nanoparticles specifically target and kill tumors with a single-dose injection, Proc. Natl. Acad. Sci. USA 111 (2014) 14900–14905.

[17] J. He, K. Fan, X. Yan, Ferritin drug carrier (FDC) for tumor targeting therapy, J. Control. Release Soc. 311–312 (2019) 288–300.

[18] C. Lv, S. Yin, X. Zhang, J. Hu, T. Zhang, G. Zhao, 16-Mer ferritin-like protein templated gold nanoclusters for bioimaging detection of methylmercury in the brain of living mice, Anal. Chim. Acta 1127 (2020) 149–155.

[19] L. Li, C.J. Fang, J.C. Ryan, et al., Binding and uptake of H-ferritin are mediated by human transferrin receptor-1, Proc. Natl. Acad. Sci. USA 107 (2010) 3505–3510.

[20] C. Cao, X. Wang, Y. Cai, et al., Targeted in vivo imaging of microscopic tumors with ferritin-based nanoprobes across biological barriers, Adv. Mater. 26 (2014) 2566–2571.

[21] L. Fiandra, S. Mazzucchelli, M. Truffi, M. Bellini, L. Sorrentino, F. Corsi, In vitro permeation of FITC-loaded ferritins across a rat blood-brain barrier: a model to study the delivery of nanoformulated molecules, JoVE (2016).

[22] K. Fan, X. Jia, M. Zhou, et al., Ferritin nanocarrier traverses the blood brain barrier and kills glioma, ACS Nano 12 (2018) 4105–4115.

[23] W. Liu, Q. Lin, Y. Fu, et al., Target delivering paclitaxel by ferritin heavy chain nanocages for glioma treatment, J. Control Release Soc. 323 (2020) 191–202.

[24] S. Gagliardi, M. Truffi, V. Tinelli, et al., Bisdemethoxycurcumin (BDC)-loaded H-ferritin-nanocages mediate the regulation of inflammation in Alzheimer's disease patients, Int. J. Mol. Sci. 23 (2022) 9237.

[25] M.A. Rizzo, R. Dal Magro, L. Barbieri, et al., H-Ferritin nanoparticle-mediated delivery of antibodies across a BBB in vitro model for treatment of brain malignancies, Biomater. Sci. 9 (2021) 2032–2042.

[26] F. Silva, L. Sitia, R. Allevi, et al., Combined method to remove endotoxins from protein nanocages for drug delivery applications: the case of human ferritin, Pharmaceutics 13 (2021) 229.

[27] F. Andreata, A. Bonizzi, M. Sevieri, et al., Co-administration of H-ferritin-doxorubicin and Trastuzumab in neoadjuvant setting improves efficacy and prevents cardiotoxicity in HER2 + murine breast cancer model, Sci. Rep. 10 (2020), 11425.

[28] H. Gomi, T. Yokoyama, S. Itohara, Role of GFAP in morphological retention and distribution of reactive astrocytes induced by scrapie encephalopathy in mice, Brain Res. 1312 (2010) 156–167.

[29] L. Li, A. Lundkvist, D. Andersson, et al., Protective role of reactive astrocytes in brain ischemia, J. Cereb. Blood Flow. Metab. J. Int. Soc. Cereb. Blood Flow Metab. 28 (2008) 468–481.

[30] M. Lorger, B. Felding-Habermann, Capturing changes in the brain microenvironment during initial steps of breast cancer brain metastasis, Am. J. Pathol. 176 (2010) 2958–2971.

[31] D.P. Fitzgerald, D. Palmieri, E. Hua, et al., Reactive glia are recruited by highly proliferative brain metastases of breast cancer and promote tumor cell colonization, Clin. Exp. Metastasis 25 (2008) 799–810.

[32] S.-J. Kim, J.-S. Kim, E.S. Park, et al., Astrocytes upregulate survival genes in tumor cells and induce protection from chemotherapy, Neoplasia 13 (2011) 286–298.

[33] F. Xing, Y. Liu, S. Sharma, et al., Activation of the c-Met pathway mobilizes an inflammatory network in the brain microenvironment to promote brain metastasis of breast cancer, Cancer Res. 76 (2016) 4970–4980.

[34] C. Choy, K.I. Ansari, J. Neman, et al., Cooperation of neurotrophin receptor TrkB and Her2 in breast cancer cells facilitates brain metastases, Breast Cancer Res. 19 (2017), 51.

[35] T.B. Terrell-Hall, M.I. Nounou, F. El-Amrawy, J.I.G. Griffith, P.R. Lockman, Trastuzumab distribution in an in-vivo and in-vitro model of brain metastasis of breast cancer, Oncotarget 8 (2017) 83734–83744.

[36] M. De Laurentiis, G. Cancello, L. Zinno, et al., Targeting HER2 as a therapeutic strategy for breast cancer: a paradigmatic shift of drug development in oncology, Ann. Oncol. J. Eur. Soc. Med. Oncol. 16 (4) (2005) iv7–iv13.

[37] O. Martínez-Sáez, A. Prat, Current and future management of HER2-positive metastatic breast cancer, JCO Oncol. Pract. 17 (2021) 594–604.

[38] D.H. Gutmann, H. Kettenmann, Microglia/Brain macrophages as central drivers of brain tumor pathobiology, Neuron 104 (2019) 442–449.

[39] S.-Y. Wu, K. Watabe, The roles of microglia/macrophages in tumor progression of brain cancer and metastatic disease, Front. Biosci 22 (2017) 1805–1829.

[40] Y. Shi, X. Fan, H. Deng, et al., Trastuzumab triggers phagocytic killing of high HER2 cancer cells in vitro and in vivo by interaction with Fcγ receptors on macrophages, J. Immunol. 194 (2015) 4379–4386.

[41] J.O. Richards, S. Karki, G.A. Lazar, H. Chen, W. Dang, J.R. Desjarlais, Optimization of antibody binding to FcgammaRIIa enhances macrophage phagocytosis of tumor cells, Mol. Cancer Ther. 7 (2008) 2517–2527.

[42] F.S. Sutterwala, G.J. Noel, P. Salgame, D.M. Mosser, Reversal of proinflammatory responses by ligating the macrophage Fcgamma receptor type I, J. Exp. Med. 188 (1998) 217–222.

[43] J. Pander, M. Heusinkveld, T. van der Straaten, et al., Activation of tumor-promoting type 2 macrophages by EGFR-targeting antibody cetuximab, Clin. Cancer Res. J. Am. Assoc. Cancer Res. 17 (2011) 5668–5673.

[44] A. Montfort, C. Dufau, C. Colacios, et al., Anti-TNF, a magic bullet in cancer immunotherapy? J. Immunother. Cancer 7 (2019), 303.

[45] A. Montfort, C. Colacios, T. Levade, N. Andrieu-Abadie, N. Meyer, B. Ségui, The TNF Paradox in Cancer Progression and Immunotherapy, Front. Immunol. 10 (2019), 1818.

[46] M.S. Ewer, S.M. Lippman, Type II chemotherapy-related cardiac dysfunction: time to recognize a new entity, J. Clin. Oncol. J. Am. Soc. Clin. Oncol. 23 (2005) 2900–2902.

[47] S. Mazzucchelli, M. Bellini, L. Fiandra, et al., Nanometronomic treatment of 4T1 breast cancer with nanocaged doxorubicin prevents drug resistance and circumvents cardiotoxicity, Oncotarget 8 (2017) 8383–8396.

[48] Y. Chen, C. Li, P. Song, et al., Hepatic and renal tissue damage in Balb/c mice exposed to diisodecyl phthalate: The role of oxidative stress pathways, Food Chem. Toxicol. Int J. Publ. Br. Ind. Biol. Res Assoc. 132 (2019), 110600.

[49] R. Toita, T. Kawano, S. Fujita, M. Murata, J.-H. Kang, Increased hepatic inflammation in a normal-weight mouse after long-term high-fat diet feeding, J. Toxicol. Pathol. 31 (2018) 43–47.

[50] O. Sánchez, A. Arnau, M. Pareja, E. Poch, I. Ramírez, M. Soley, Acute stress-induced tissue injury in mice: differences between emotional and social stress, Cell Stress Chaperones 7 (2002) 36–46.

[51] M.N. Mills, W. King, A. Soyano, et al., Evolving management of HER2+ breast cancer brain metastases and leptomeningeal disease, J. Neurooncol 157 (2022) 249–269.

[52] H.J. Stemmler, S. Kahlert, W. Siekiera, M. Untch, B. Heinrich, V. Heinemann, Characteristics of patients with brain metastases receiving trastuzumab for HER2 overexpressing metastatic breast cancer, Breast Edinb. Scotl. 15 (2006) 219–225.